9-2015

Stability and Decomposition of Ca-Substituted Lanthanum Ferrite in Reducing Atmospheres

Patrick M. Price
Boise State University

Darryl P. Butt
Boise State University

J. Am. Ceram. Soc., 98 [9] 2881–2886 (2015)
DOI: 10.1111/jace.13569

journal

Stability and Decomposition of Ca-Substituted Lanthanum Ferrite in Reducing Atmospheres

Patrick M. Price,[‡] and Darryl P. Butt[‡,§,†]

[‡]Department of Materials Science and Engineering, Boise State University, 1910 University Dr., Boise, Idaho 83725

[§]Center for Advanced Energy Studies, 995 University Boulevard, Idaho Falls, Idaho 83401

Calcium-substituted lanthanum ferrites ($La_{1-x}Ca_xFeO_{3-\delta}$ $x = 0, 0.1, 0.2, 0.3, 0.4$) were synthesized in air and subsequently decomposed in reducing atmospheres. The partial pressure of oxygen (P_{O_2}) was controlled by varying the H_2/H_2O ratio by bubbling hydrogen/argon mixtures through water baths at controlled temperatures. Three regions of mass loss were identified as the P_{O_2} was reduced, two of which were determined to be associated with decomposition reactions. Calcium was shown to decrease the thermal stability of the perovskite compound, but rather than incrementally increasing the required P_{O_2} for decomposition proportional to calcium concentration, all samples partially decomposed at a single P_{O_2}. The extent of the partial decomposition was dependent on the amount of calcium substitution and temperature. The perovskite phase remaining after the partial decomposition was found to fully decompose at the same oxygen partial pressure as pure lanthanum ferrite.

I. Introduction

There is a strong motivation to develop new technologies that can sustainably supplement world energy requirements and reduce carbon emissions. One such technology is the utilization of ion conducting ceramic oxide membranes for use in high-temperature electrochemical devices for energy conversion such as the solid oxide fuel cell, the conversion of natural gas into synthesis gas (syngas), oxidation of other hydrocarbons, hydrogen and oxygen production, and hybrid energy systems.[1–5] Syngas reactors can be used in conjunction with other technologies for onsite production of easily transportable liquid products from natural gas that would otherwise be flared at remote oil extraction facilities. Calcium-substituted lanthanum ferrite materials (LCF) have been shown to be suitable candidates as oxygen transport membranes in syngas reactors due to the combination of excellent stability at high temperatures under reducing conditions and high oxygen flux rates.[6]

Lanthanum ferrite ($LaFeO_3$) has the orthorhombic, Pbnm, ABO_3 perovskite structure as shown in Fig. 1.[7] When Ca^{2+} is added it to lanthanum ferrite it forms a solid solution by occupying the La^{3+} A site. In addition to the small difference in ionic radii (~3%), the difference in valance results in a charge imbalance.[8] As a result, there are two possible charge compensating mechanisms: either an oxygen vacancy may form for every two Ca^{2+} ions added, or the valence state of iron may change from Fe^{3+} to Fe^{4+}. The extent to which each of these compensation mechanisms occurs is affected by the thermal history and partial pressure of oxygen during synthesis or sustained annealing of the material. Synthesizing samples under low oxygen partial pressures will result in charge compensation primarily by the formation of oxygen vacancies as confirmed by Mossbauer spectroscopy[9,10] Previous studies have reported the simultaneous existence of both oxygen vacancies and tetravalent iron in LCF samples treated in air.[11,12] A solubility limit exists in the LCF system, after which adding more calcium will result in secondary phases. The secondary phases have a crystal structure almost identical to the perovskite structure, and can be considered an oxygen deficient perovskite with ordered oxygen vacancies in the [110] direction of the *Pbnm* structure as shown in Fig 1. This similarity in crystal structure allows for the formation of intergrowth structures, which are the uninterrupted stacking of the two phases along the [001] direction, which are analogous to a stacking fault rather than crystallites of two distinct phases.

When iron based perovskite materials are subjected to sufficiently reducing atmospheres at elevated temperatures, a large mass loss is observed as the material decomposes. A study by Nakamura *et al.*[13] investigated the decomposition behavior of lanthanum ferrite at 1000°C and 1200°C and has shown that $LaFeO_3$ decomposes in the following reaction:

$$LaFeO_3 \rightarrow \frac{1}{2}La_2O_3 + Fe + \frac{3}{4}O_2 \quad (1)$$

Despite great interest in syngas materials, decomposition partial pressures have not been reported for calcium-substituted lanthanum ferrites near the expected operating temperatures of the membranes (~750°C–900°C). In this study, we synthesized LCF materials with 0%, 10%, 20%, 30%, and 40% calcium substitution and have investigated the decomposition behavior of each composition under reducing atmospheres at 800°C, 900°C, and 1000°C.

II. Experimental Procedures

Lanthanum calcium ferrites were synthesized using the procedures discussed previously.[14] The orthorhombic (*Pbnm*) structure of synthesized samples was verified using a X-ray diffractometer (Bruker AXS D8, Madison, WI) with parallel beam geometry at room temperature. Differential scanning calorimetry (DSC) and thermogravimetric analysis (TGA) were used to investigate the thermal stability of LCF compounds in reducing atmospheres. All thermal analysis studies were performed in a thermal analyzer (Netszch STA-449, Burlington, MA) equipped with a simultaneous DSC and TGA (DSC/TG) carrier, silicon carbide furnace, alumina protective tube, and 85 μL platinum rhodium (Pt/Rh) crucibles. Temperature calibrations were performed by the melting of five pure metals. To remove background and noise from the sample signal, correction files were created prior to all thermal analysis experiments by running the DSC/TGA stage

T. M. Besmann—contributing editor

Manuscript No. 35496. Received August 20, 2014; approved February 17, 2015.
[†]Author to whom correspondence should be addressed. e-mail: darrylbutt@boisestate.edu

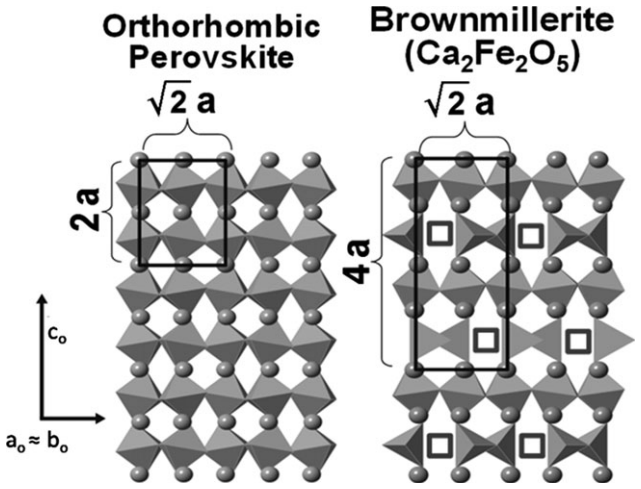

Fig. 1. The LCF perovskite structure is composed of large A-site cations, Fe cations located at the center of each octahedra, and oxygen atoms located at the vertices of the octahedra. Ordered oxygen vacancies may form along the [110] direction transforming octahedra to tetrahedra as indicated by the squares in the brownmillerite structure shown above.

with empty crucibles using equivalent parameters as sample measurements. An empty Pt/Rh crucible was used as a reference for all sample measurements. All samples were ramped at 20°C/min with a total gas flow rate of 200 mL/min. Reducing atmospheres were achieved using certified H_2–Ar gas mixtures (2% or 6% H_2; balance Argon) with a measured moisture content of less than 10 ppm. The DSC/TGA has three internal mass flow controllers (MFC). Two of the MFCs are available for experiments and one is used to provide a continuous flow of 10 mL/min of high-purity argon (99.999%) protective gas through the balance chamber. Each MFC was adjusted for the appropriate gas densities. The argon gas was passed through a gas purifier (Sigma-Aldrich Supleco 22398, St. Louis, MO) operating at 580°C to remove any residual oxygen. The resulting oxygen partial pressure was measured with a zirconia cell oxygen analyzer (Neutronics OA-1, Exton, PA) operating at 725°C. A nominal voltage reading of 570 mV was recorded correlating to approximately $P_{O_2} = 10^{-12}$ bar. The P_{O_2} was calculated using the Nernst equation as follows:

$$\text{Electrical Potential}(V) = \frac{RT}{nF}\ln\left(\frac{0.209}{\text{Unknown}P_{O_2}}\right) \tag{2}$$

Required oxygen partial pressures can be produced by varying the ratio of H_2 and H_2O in the atmosphere for a given temperature. In these experiments, oxygen partial pressures were achieved by controlling the volume ratio of experimental gases with MFC. The total gas flow through the sample chamber was held constant for the duration of all experiments and it should be noted that the oxygen partial pressure is determined by the combined H_2/H_2O ratio of the two gas streams, rather than the flow rate itself. The experimental gases were mixed in a manifold and passed through a section of stainless steel tubing to facilitate mixing prior to entering the experimental chamber. The certified H_2–Ar gas mixture was delivered to the MFC either directly from the cylinder or bubbled through a water bath at controlled temperature and pressure. The pressure above the water bath was measured with a calibrated test pressure gauge with a ±0.5% accuracy (OMEGA Engineering PGT-30L-15, Stamford, CT) and controlled with a precision pressure regulator (±0.05% precision) (OMEGA Engineering Omega PRG101-25, Stamford, CT). All gas lines and fittings were welded or fitted with stainless steel fittings (Swagelok, Solon, OH) to limit hydrogen or oxygen leakage. The hydrogen bubbler apparatus is shown in Fig. 2. The bubbler water was contained in a glass beaker placed inside an insulated dewar, surrounded by a copper coil, and immersed in a circulated water bath, which was held at 0.5°C by an external cooling unit. The dewar was placed in a 2″ foam lined box for added thermal stability. A K-type thermocouple was inserted directly into the bubbler water bath and the temperature was continuously monitored with a digital thermometer (OMEGA Engineering HH806AW, Stamford, CT). The stainless steel gas line feeding the bubbler was precooled by a copper line from the external cooling unit and all cooling and gas lines were insulated.

The partial pressure of the system can be calculated using thermodynamic relationships for the following chemical reaction:

$$2H_2 + O_2 \rightarrow 2H_2O \tag{3}$$

The equilibrium constant, K, for the formation of water vapor can be calculated using the Gibbs free energy of formation ΔG as shown in the following two equations:

$$K = \frac{(P_{H_2O})^2}{(P_{H_2})^2(P_{O_2})} \tag{4}$$

$$K = \exp^{\left(\frac{-\Delta G}{RT}\right)} \tag{5}$$

Solving for the partial pressure of oxygen from Eqs. (4) and (5) gives:

$$P_{O_2} = \left(\frac{P_{H_2}}{P_{H_2O}}\right)^{-2} \exp^{\left(\frac{-\Delta G}{RT}\right)}(\text{bar}) \tag{6}$$

The Gibbs free energy of formation was taken from the JANAF tables for temperatures from 1000 to 1400 K and a linear fit was applied to extrapolate intermediate values given in the following equation:

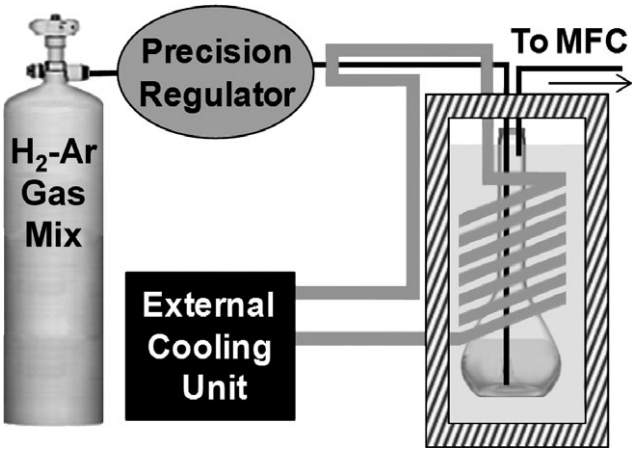

Fig. 2. A schematic of the hydrogen gas bubbler apparatus used to control the P_{H_2O} and P_{O_2}. Hydrogen/argon gas mixtures were bubbled through a thermally stable water bath in a flask with controlled pressure and flow rate. The flask was surrounded by a water bath in an insulated dewar, which was also insulated by an additional 2 inches of foam board. The water surrounding the flask was circulated with a small pump to avoid thermal gradients and was actively chilled by an external cooling unit coil which also precooled the stainless steel gas line.

$$\Delta G_{H_2O(g)} = 112.522(T) - 497790.8(\text{J/mol}) \quad (7)$$

The pressure of water vapor (P_{H_2O}) above the water bath was calculated from the ITS-90 formulations for vapor pressure using the following equation.[15]

$$\ln(e_s) = \sum_{i=0}^{6} g_i T^{i-2} + g_7 \ln(T)(\text{Pa}) \quad (8)$$

where, $g_0 = -2.8365744 \times 10^3$, $g_1 = -6.028076559 \times 10^3$, $g_2 = 1.954263612 \times 10^1$, $g_3 = -2.737830188 \times 10^{-2}$, $g_4 = 1.6261698 \times 10^{-5}$, $g_5 = 7.0229056 \times 10^{-10}$, $g_6 = -1.8680009 \times 10^{-13}$, and $g_7 = 2.7150305$.

The partial pressure of hydrogen (P_{H_2}) above the water bath can be calculated as a function of the line pressure exerted by the pressure regulator (LP), the atmospheric pressure (ATM), the partial pressure of water vapor as a function of temperature from Eq. (8), the back pressure exerted by the water above the bottom of the submerged inlet tube (WBP), and the hydrogen concentration in the H_2–Ar mixture as given in Eq. (9). Typically, the line pressure was held at 4 psi, the water head was 6 cm and the average daily atmospheric pressure was 92 kPa giving a total pressure of approximately 120 kPa.

$$P_{H_2}(T) = (\text{ATM} = \text{LP} - e_s(T) - \text{WBP}) * [H_2](\text{Pa}) \quad (9)$$

The water vapor partial pressure is equal to e_s from Eq. (8) for bubbled gases and can be directly calculated from the measured moisture content in the tank for dry gas. The total H_2/H_2O ratio of two mixed gases with predetermined MFC gas flow rates (P1 and P2) can be calculated from the following equation:

$$\left(\frac{P_{H_2}}{P_{H_2O}}\right)_{\text{Total}} = \frac{P_{H_2}(T1)\frac{P_1}{P_1+P_2} + P_{H_2}(T2)\frac{P_1}{P_1+P_2}}{P_{H_2O}(T1)\frac{P_1}{P_1+P_2} + P_{H_2O}(T2)\frac{P_1}{P_1+P_2}} \quad (10)$$

The total experimental partial pressure of oxygen in the unit bar can then be calculated by combining Eqs. (7) and (11) giving the following equation:

$$P_{O_2} = \left(\frac{P_{H_2}(T1)\frac{P_1}{P_1+P_2} + P_{H_2}(T2)\frac{P_1}{P_1+P_2}}{P_{H_2O}(T1)\frac{P_1}{P_1+P_2} + P_{H_2O}(T2)\frac{P_1}{P_1+P_2}}\right)^{-2} e^{\frac{754672.4}{598738}}(\text{bar}) \quad (11)$$

Table I lists the gas mixtures used and calculated range of achievable oxygen partial pressures at each experimental temperature.

Table I. List of Experimental Gas Mixtures and Bath Temperatures Used to Control Oxygen Partial Pressure

% H_2	Isothermal temperature (°C)	Dry	Bubbled 0.5°C	Bubbled 22.5°C
		Log [P_{O2}] (bar)		
2%	800	−26.95	−19.5	−18.21
	900	−24.89	−17.43	−16.15
	1000	−23.15	−15.69	−14.47
6%	800	−27.91	−20.45	−19.17
	900	−25.84	−18.39	−17.1
	1000	−24.1	−16.65	−15.36

III. Results and Discussion

Previous studies have shown that pure $LaFeO_3$ decomposes into iron, lanthanum oxide, and oxygen in sufficiently reducing atmospheres.[13] The data in Fig. 3 show mass loss for the complete decomposition of the Ca-substituted samples (0%–40% Ca) isothermally treated in 6%H_2/94% Ar at 1100°C. These mass losses are consistent with the formation of calcium oxide (CaO), lanthanum oxide (La_2O_3), and iron. Peaks associated with all three phases were present in X-ray diffraction data. Therefore, decomposition of LCF is given by the following equation:

$$La_{1-x}Ca_xFeO_{3-\delta} \rightarrow \frac{1-x}{2}La_2O_3 + xCaO + Fe + \frac{3-x}{4}O_2 \quad (12)$$

The measured mass losses were within 0.25% of the theoretical value except for the 40% Ca-substituted sample, which was within 0.5% of theoretical values. Previous studies have shown that a small percentage of ordered oxygen vacancies exist at this high Ca concentration, which would decrease the amount of available oxygen for decomposition.[14]

Examples of decomposition curves for LCF samples treated at 1000°C are shown in Fig. 4. A typical thermal profile and gas flow rate scheme is also shown. The data show three distinct mass loss regions labeled LR1, LR2, and LR3 as the partial pressure of oxygen is reduced. All samples were chemically stable during the initial ramp to 500°C in 200 mL/min of purified Ar with a $P_{O_2} \approx 10^{-12}$ bar. At 500°C, the $P_{O_2}$was decreased by switching the gas to moist (0.5°C bath) 6% H_2, resulting in mass loss. A 30 min isotherm was evoked to ensure complete oxygen evolution at this stage, which will be referred to as mass loss region #1 (LR1). The furnace temperature was increased to 1000°C while continuing to flow moist gas. Calcium-substituted samples began to decompose when the furnace reached 1000°C at $P_{O_2} = 10^{-16.65}$ bar. The rapid mass loss continued for a short period of time, after which, the rate of decomposition slows, but does not stop. This part of the decomposition curve will be referred to as mass loss region #2 (LR2).

The oxygen partial pressure is further reduced during the isotherm by introducing a dry 6%H_2 gas stream, which

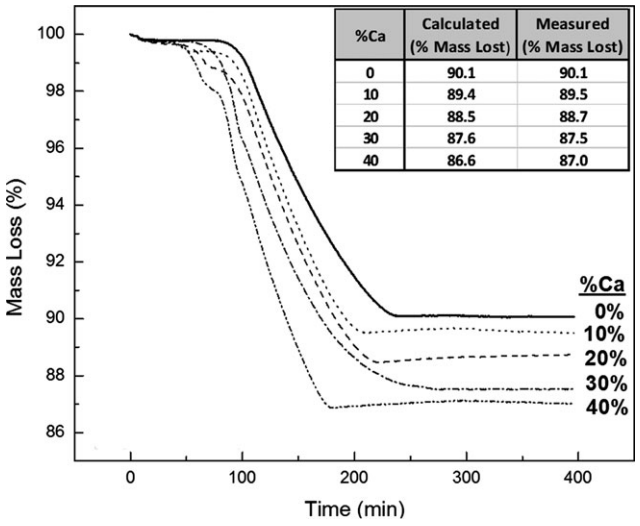

Fig. 3. Thermogravimetric data showing the mass loss kinetics to full decomposition in 6% H_2 at 1100°C. The mass loss was consistent with the formation of CaO, La_2O_3, and metallic Fe, with a maximum deviation of less than 0.5% from theoretical values shown in the inset.

begins to decompose the sample in mass loss region #3 (LR3). The oxygen partial pressure was incrementally increased by decreasing the fraction of dry 6% H_2 gas. As the P_{O_2} was increased the rate of decomposition decreased until the equilibrium partial pressure of the decomposition reaction was achieved, after which, further increasing the P_{O_2} resulted in oxidation with an observed increase in mass indicating that the decomposition reaction is reversible. Equilibrium oxygen partial pressures for the decomposition reaction were calculated using the H_2/H_2O ratios at the onset of oxidation.

A separate experiment with increased P_{O_2} was required to find equilibrium oxygen partial pressure for the decomposition reaction in LR2. Though not shown here, the decomposition behavior in LR2 followed the same reversible behavior as LR3 described above and shown in Fig. 3.

No change in mass was observed for $LaFeO_3$ in LR1 and LR2 at any temperature. There was also no change in mass in LR2 for the 10% Ca-substituted sample at 800°C or 900°C, but a small mass loss was observed at 1000°C. In the following, we attempt to give a physical explanation for the occurrence of mass loss in each of the three mass loss regions.

The mass loss observed in LR1 is wholly consistent with the formation of oxygen vacancies, assuming that initially calcium-substituted samples are entirely charge compensated by Fe^{4+}, which is then reduced to Fe^{3+}. The ionic radius of the Fe^{3+} cation is 18% larger than Fe^{4+} resulting in expansion of the material.[8,16] X-ray diffraction patterns of specimens isothermally treated at 500°C in LR1 shift to lower angles, which are consistent with the expected chemical expansion due to the change in iron valance. Rietveld refinement was used to quantify the chemical expansion of the perovskite unit cell as a function of calcium composition before and after reduction in LR1, which is shown in Fig 5.

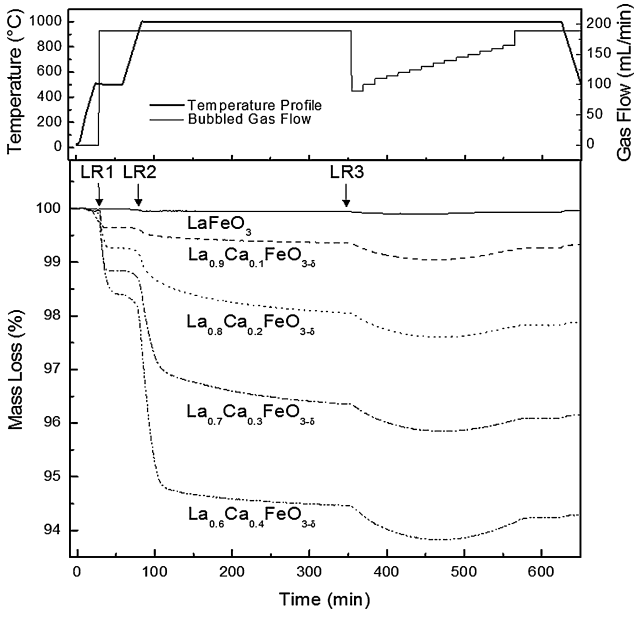

Fig. 4. Decomposition behavior of calcium-doped lanthanum ferrites as a function of composition at 1000°C. The temperature was initially held at 500°C to ensure complete oxygen disassociation in the first mass loss region (LR1). When the temperature was increased to 1000°C at a partial pressure of $10^{-16.64}$ bar, rapid decomposition was observed in all five materials, that is, in the second mass loss region (LR2), followed by a slow linear mass loss. The oxygen partial pressure was then decreased to $10^{-17.30}$ bar after which all materials, including $LaFeO_3$, began to decompose in the final mass loss region (LR3). The partial pressure was then increased in a stepwise fashion back to $10^{-16.64}$ bar. The reversible reaction begins to reoxidize the materials at a partial pressure of $10^{-16.98}$ resulting in weight gain as indicated by the thermogravimetric data.

No calcium oxide, iron, or ordered oxygen vacancy structures were observed in the XRD data of samples reduced in LR1.

The reversible decomposition behavior of $LaFeO_3$, which only occurs in LR3, is consistent with the findings of Nakamura *et al.*[13] The equilibrium partial pressure of oxygen at 1000°C was calculated to be $10^{-16.98}$ bar using the double gas flow method described here. This is very close to the equilibrium oxygen partial pressure of $10^{-16.95}$ bar reported by Nakamura *et al.* Calcium-substituted samples were allowed to reach a semisteady state in LR2 prior to decomposition in LR3. Rather than a progressive shift dependent on calcium concentration, all compositions were found to decompose at the exact same equilibrium P_{O_2} in LR3.

The chemically invariant nature of the decomposition P_{O_2} in LR3 indicates a single chemical reaction with a single value of standard free energy given by the following equation, where ¾ is the stoichiometric fraction of O_2 produced in the reaction.

$$\Delta G^\circ = -RT\ \ln(K) = -\frac{3}{4}RT\ 2.303\mathrm{Log}[P_{O_2}]\ \mathrm{J/mol} \quad (13)$$

The standard enthalpy and entropy can be estimated using the following equations:

$$\Delta H^\circ = \left(\frac{\Delta G_1^\circ}{T_1} - \frac{\Delta G_2^\circ}{T_2}\right) \Big/ \left(\frac{1}{T_1} - \frac{1}{T_2}\right)\ \mathrm{J/mol} \quad (14)$$

$$\Delta S^\circ = \frac{\Delta G_1^\circ - \Delta G_2^\circ}{T_1 - T_2} \quad (15)$$

The measured equilibrium oxygen partial pressure for LR3 and thermodynamic estimations are listed in Table II.

Similar to LR3, the mass lost in LR2 was recovered with increasing P_{O_2}. The equilibrium P_{O_2} for the decomposition reaction in LR2 was approximately two orders of magnitude higher than LR3 as indicated in Table II. Similar to LR3, the measured equilibrium P_{O_2} for the decomposition reaction in LR2 was equal for all specimens at a given temperature and was not dependent on composition. However, the amount of mass lost in LR2 was found to be proportional to the calcium concentration. The percentage of calcium decomposed to CaO in LR2 is given in Table III. The data indicate

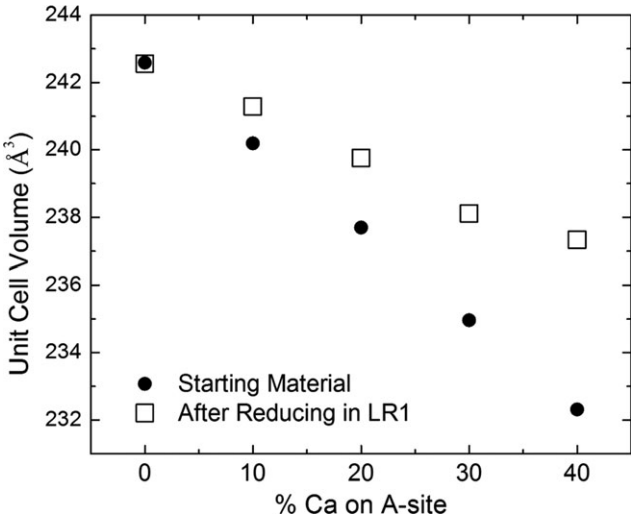

Fig. 5. Rietveld refinement of XRD data shows the volume expansion of the perovskite unit cell as a result of both the transformation of $Fe^{3+} \rightarrow Fe^{4+}$ and the formation of oxygen vacancies in mass loss region #1 (LR1).

Table II. Equilibrium P_{O_2} values corresponding to the observed decomposition in LR1 and LR2

	Isotherm (°C)	% H_2	Gas Stream #1	Flow #1 (mL/min)	Gas Stream #2	Flow #2 (mL/min)	Log [P_{O2}] (Bar)	$\Delta G°$ (kJ/mol)	$\Delta H°$ (kJ/mol)	$\Delta S°$ [J·(mol·K)$^{-1}$]
Decomposition of $Ca_2Fe_2O_5$	800						−19.6	302	425	−114
	900						−17.3	291		
LR2	800	6%	0.5°C	110	22.5°C	80	−19.5	301	425	−116
	900	6%	0.5°C	30	22.5°C	160	−17.2	290		
	1000	2%	0.5°C	145	22.5°C	45	−15.2	278		
LR3	800	6%	Dry	150	0.5°C	40	−21.8	336	474	−128
	900	6%	Dry	110	0.5°C	80	−19.1	322		
	1000	6%	Dry	60	0.5°C	130	−17.0	310		

Data from Kharton *et al.*[21] for the decomposition of brownmillerite ($Ca_2Fe_2O_5$) are included for comparison. Estimated values of the standard Gibbs free energy, enthalpy, and entropy were calculated from Eqs. (13–15).

Table III. Changes in Calcium Concentrations Due to Decomposition in LR2

Starting %Ca Temperature	%Ca decomposed to CaO				Estimated %Ca left in solution			
	10	20	30	40	10	20	30	40
800°C	0.0	9.2	20.5	31.6	10.0	10.8	9.5	8.4
900°C	0.0	11.1	22.7	34.3	10.0	8.9	7.3	5.7
1000°C	5.3	15.2	26.0	36.6	4.7	4.8	4.0	3.4

that for all compositions a portion of the calcium remains in solid solution with perovskite structure. The estimated fraction of calcium left in solid solution decreases with increasing temperature. The 10% Ca sample did not show any signs of decomposition in LR2 at lower temperatures, but did show a small decomposition in LR2 at 1000°C. Table III suggests that at 1000°C less than 5% of calcium is estimated to be left in solution.

A 30% Ca-substituted specimen was annealed at 900°C for 8 h below the decomposition P_{O_2} in LR2, but above the decomposition P_{O_2} found in LR3 The x-ray diffraction pattern in Fig. 6 shows that after decomposition the 30% specimen was composed of LCF perovskite, CaO, and metallic iron. No La_2O_3 or ordered oxygen vacancy structures were found indicating almost all mass loss observed in LR2 was due to the decomposition of CaO and α-Fe. The same 30% Ca sample was reoxidized at 900°C above the decomposition P_{O_2} in LR2, but below the oxygen disassociation P_{O_2} observed in LR1. Almost all of the mass lost during the decomposition reaction was regained upon oxidation. The XRD diffraction pattern of the reoxidized sample shows the disappearance of the CaO and iron peaks confirming the reversal of the decomposition. However, additional diffraction peaks indicate a portion of the specimen oxidized to a vacancy ordered brownmillerite type phase rather than reverting back to the perovskite.

The peculiar decomposition behavior of LCF compounds can be explained by the ordering of oxygen vacancies in the perovskite structure. Calcium-substituted lanthanum ferrites decompose at discrete oxygen partial pressures in LR2 and LR3, rather than a progressive chemical-dependent shift, because the material is not single phase at the submicrometer scale under reducing conditions. Multiple studies that have reported the coexistence of brownmillerite with perovskite on this scale.[17–19] These small domains can be difficult to observe in diffraction data due to the small coherent scattering domains.[20] After the oxygen disassociation in LR1, there are enough oxygen vacancies created to reduce all of the Ca in the material from $CaFeO_3$ to $CaFeO_{2.5}$, which is the composition of the vacancy ordered brownmillerite. The extent to which the material is decomposed in LR2 at a given temperature is dependent on the ability of calcium ions to cluster and form domains of ordered oxygen vacancies. The probability that enough calcium will be available to form a domains of brownmillerite increases with increasing Ca content and temperature. This is consistent with the rapid decrease in mass shown in Fig. 4 during the initial stages of LR2 due to statistical clustering of calcium, which saturates as those regions are decomposed. This is followed by a semi-linear decomposition at a substantially reduced rate, which could be the result of calcium migration to vacancy clusters via a diffusion-controlled process. It was shown in Fig. 6 that

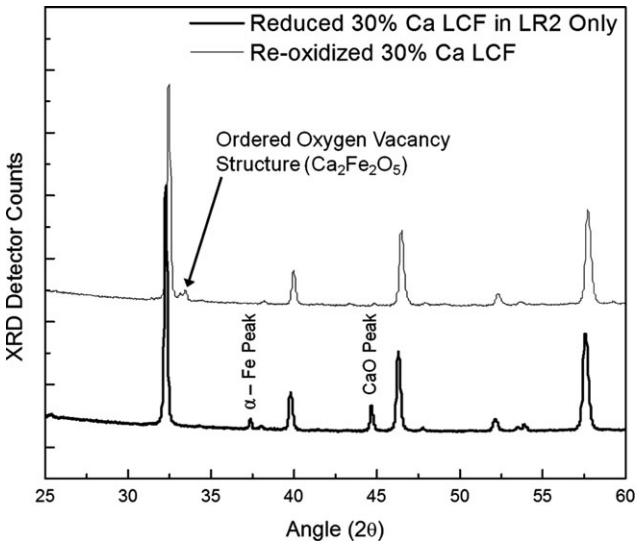

Fig. 6. X-ray diffraction patterns of a $La_{0.7}Ca_{0.3}FeO_{3-\delta}$ specimen, which was partially decomposed at 900°C in LR2, quenched for XRD analysis, and then subsequently reoxidized using a higher oxygen partial pressure. An oxygen partial pressure ($P_{O_2} = 10^{-18.4}$ bar) was selected to be low enough to achieve the partial decomposition observed in LR2, but high enough to avoid decomposition in LR3. After decomposing in LR2 both calcium oxide and metallic iron peaks are observed in the XRD spectrum. The specimen was then reoxidized above the LR2 equilibrium oxygen partial pressure ($P_{O_2} = 10^{-17.22}$ bar). The CaO and α-Fe peaks are not observed in the XRD spectrum of the reoxidized sample. However, peaks indicative of an ordered oxygen vacancy structures are present.

when the 30% Ca specimen was reoxidized, diffraction peaks correlating to ordered oxygen vacancy structures appeared. Furthermore, we have compared equilibrium P_{O_2} values for the decomposition reaction of brownmillerite ($Ca_2Fe_2O_5$) from literature to our values measured in LR2.[21] The data in Table II show that the equilibrium P_{O_2} for the decomposition reactions in LR2 are almost identical to values found in literature, supporting the claim that it is the submicrometer domains of the brownmillerite structure that is being decomposed in LR2. It should be noted that the reversibility observed in LR2 is the reduction and oxidation of the small domains of the brownmillerite structure rather than the perovskite structure, which is stable in LR2. This result suggests that as long as Ca is randomly distributed throughout the perovskite structure, the stability in reducing atmospheres will be almost equivalent to that of $LaFeO_3$ as is the case with the 10% Ca-substituted samples up to 900°C. Transversely, when calcium starts to cluster in reducing atmospheres the thermodynamically favorable ordered oxygen vacancy structure will form, which will then be susceptible to decomposition at two orders of magnitude higher oxygen partial pressures.

IV. Conclusions

The behavior of calcium-substituted lanthanum ferrite (LCF) perovskites in reducing atmospheres and elevated temperatures was investigated. Thermogravimetric data indicated that LCF materials undergo a series of three mass changes as the oxygen partial pressure (P_{O_2}) is reduced at a given temperature. Different mechanisms have been attributed to the mass loss observed in each P_{O_2} region.

The first mass loss region (LR1), which occurs at the highest P_{O_2}, is attributed to the conversion of iron valance from $Fe^{4+} \rightarrow Fe^{3+}$ with an associated oxygen vacancy formation and chemical expansion. The fraction of mass lost in LR1 indicates LCF materials synthesized in air are almost entirely charge compensated by Fe^{4+}.

The subsequent two mass loss regions (LR2 & LR3) are the result of two different decomposition reactions occurring at two discrete oxygen partial pressures for a given temperature. The equilibrium P_{O_2} for the decomposition reactions in LR2 and LR3 were not found to be dependent on the calcium concentration in the material. The decomposition in LR2 is the result of a multistep process. Oxygen vacancies form as a result of the reducing atmosphere. When enough oxygen vacancies and calcium cluster they order to form small brownmillerite ($Ca_2Fe_2O_5$) domains, which exist as intergrowths in the perovskite matrix. The mass loss observed in LR2 is a result of the decomposition of small brownmillerite domains into CaO and α-Fe. The fraction of brownmillerite formed, and thus the amount of mass lost in LR2, is dependent on the calcium concentration. The stability of the LCF perovskite structure in reducing conditions is dependent on the ability of the Ca to remain randomly distributed. This randomness is achieved by the 10% Ca-substituted compound up to 900°C, but is reduced to approximately 5% Ca at 1000°C. Greater than 10% calcium concentrations may be stable at lower temperatures. The mass loss observed in LR3 is due to the complete decomposition of the perovskite regardless of calcium concentration, including the complete decomposition of $LaFeO_3$.

The reactions in both LR1 and LR3 were found to be reversible when oxygen partial pressure was increased. The mass lost in LR2 was also regained with increasing oxygen partial pressure; however, XRD data revealed that calcium clusters oxidize to reform brownmillerite in addition to perovskite.

Calcium-substituted lanthanum ferrites have many potential applications as high-temperature oxygen conducting membranes. The equilibrium oxygen partial pressures and decomposition behavior discussed here can be used to help design and determine the operation limitations of these materials.

References

[1]U. Balachandran, J. T. Dusek, R. L. Mieville, R. B. Poeppel, M. S. Kleefisch, S. Pei, T. P. Kobylinski, C. A. Udovich, and A. C. Bose, "Dense Ceramic Membranes for Partial Oxidation of Methane to Syngas," *Appl. Catal. A*, **133** [1] 19–29 (1995).

[2]J. A. Kilner, "Optimisation of Oxygen Ion Transport in Materials for Ceramic Membrane Devices," *Faraday Discuss.*, **134**, 9–15 (2007).

[3]P. S. Maiya, U. Balachandran, J. T. Dusek, R. L. Mieville, M. S. Kleefisch, and C. A. Udovich, "Oxygen Transport by Oxygen Potential Gradient in Dense Ceramic Oxide Membranes," *Solid State Ionics*, **99** [1–2] 1–7 (1997).

[4]V. V. Kharton, A. A. Yaremchenko, A. V. Kovalevsky, A. P. Viskup, E. N. Naumovich, and P. F. Kerko, "Perovskite-Type Oxides for High-Temperature Oxygen Separation Membranes," *J. Membr. Sci.*, **163** [2] 307–17 (1999).

[5]P. V. Hendriksen, P. H. Larsen, M. Mogensen, F. W. Poulsen, and K. Wiik, "Prospects and Problems of Dense Oxygen Permeable Membranes," *Catal. Today*, **56** [1–3] 283–95 (2000).

[6]P. N. Dyer, M. F. Carolan, D. Butt, R. H. E. V. Dooorn, and R. A. Cutler, Air Products and Chemicals Inc, "Mixed Conducting Membranes for Syngas Production," U.S. Patent No. 6,492,290, August 2002.

[7]M. Marezio and P. D. Dernier, "The Bond Lengths in LaFeO3," *Mater. Res. Bull.*, **6** 23–30 (1971).

[8]R. D. Shannon and C. T. Prewitt, "Effective Ionic Radii in Oxides and Flourides," *Acta Crystallogr. Sect. B-Struct. Crystallogr. Cryst. Chem.*, **25**, 925–46 (1969).

[9]J. C. Grenier, L. Fournes, M. Pouchard, P. Hagenmuller, and S. Komornicki, "Mossbauer Resonance Studies on the $Ca_2Fe_2O_5$-$LaFeO_3$ System," *Mater. Res. Bull.*, **17** [1] 55–61 (1982).

[10]S. Komornicki, L. Fournes, J. C. Grenier, F. Menil, M. Pouchard, and P. Hagenmuller, "Investigation of Mixed Valency Ferrites $La_{1-x}Ca_xFeO_{3-y}$ ($0<x<0.50$) with the Perovskite Structure," *Mater. Res. Bull.*, **16** [8] 967–73 (1981).

[11]H. Taguchi, Y. Masunaga, K. Hirota, and O. Yamaguchi, "Synthesis of Perovskite-Type $(La_{1-X}Ca_x)FeO_3$ ($0 \le x \le 0.2$) at Low Temperature," *Mater. Res. Bull.*, **40**, 773–80 (2005).

[12]P. Ciambelli, S. Cimino, L. Lisi, M. Faticanti, G. Minelli, I. Pettiti, and P. Porta, "La, Ca and Fe Oxide Perovskites: Preparation, Characterization and Catalytic Properties for Methane Combustion," *Appl. Catal. B*, **33** [3] 193–203 (2001).

[13]T. Nakamura, G. Petzow, and L. J. Gauckler, "Stability of the Perovskite Phase $LaBO_3$ (B = V, Cr, Mn, Fe, Co, Ni) in Reducing Atmosphere," *Mater. Res. Bull.*, **14**, 649–59 (1979).

[14]P. M. Price, E. Rabenberg, D. Thomsen, S. T. Misture, and D. P. Butt, "Phase Transformations in Calcium-Substituted Lanthanum Ferrite," *J. Am. Ceram. Soc.*, **97**, 2241–8 (2014).

[15]B. Hardy, *ITS-90 Formulations for Vapor Pressure, Frostpoint Temperature, Dewpoint Temperature, and Enhancement Factors in the Range −100 to +100°C*. Thunder Scientific Corporation, Albuquerque, NM, 1998.

[16]S. B. Adler, "Chemical Expansivity of Electrochemical Ceramics," *J. Am. Ceram. Soc.*, **84**, 2117–9 (2001).

[17]T. C. Gibb, "An Investigation of Microdomains in $Ca_2LaFe_3O_8$ by Mossbauer Spectroscopy," *J. Solid State Chem.*, **74**, 176–83 (1988).

[18]J. M. Gonzalez-Calbet, M. Vallet-Regi, and J. Alonso, "Nonstoichiometry and Structural Intergrowth in the $CaFe_xMn_{1-x}O_{3-y}$ ($0 \le x \le 1$) System," *J. Solid State Chem.*, **71**, 331–41 (1987).

[19]M. A. Alario-Franco, M. Vallet-Regi, and J. M. Gonzalez-Calbet, "Nonstoichiometry and Disordered Intergrowth in Anion-Deficient Perovskites," *Cryst. Lattice Defects Amorphous Mater.*, **16** [1–4] 387–94 (1987).

[20]S. V. Cherepanova and S. V. Tsybulya, "Peculiarities of the X-ray Diffraction of Oxygen-Deficient Perovskite-Related Materials with Partial Vacancy Ordering," *Z. Kristallorg. Suppl.*, **27**, 5–12 (2008).

[21]V. V. Kharton, E. V. Tsipis, V. A. Kolotygin, M. Avdeev, A. P. Viskup, J. C. Waerenborgh, and J. R. Frade, "Mixed Conductivity and Stability of $CaFe_2\ O_{4-\delta}$," *J. Electrochem. Soc.*, **155**, P13 (2008). □